

## RESEARCH ARTICLE OPEN ACCESS

# High Strength Anhydrite Cement Based on Lime Mud From Water Treatment Process: One Step Synthesis in Water Environment, Characterization and Technological Parameters

Maksim Kamarou<sup>1</sup> | Hongbin Tan<sup>2</sup> | Dmitry Moskovskikh<sup>3</sup> | Natallia Kulinich<sup>4</sup> | Xiaoling Ma<sup>2</sup> | Feihua Yang<sup>5</sup> | Evgenii Beletskii<sup>6</sup> | Elena Alekseeva<sup>6</sup> | Sergey Yudin<sup>7</sup> | Valentin Romanovski<sup>8</sup> 

<sup>1</sup>International Information and Analytical Center for Technology Transfer, Belarusian State Technological University, Minsk, Belarus | <sup>2</sup>School of Materials and Chemistry, Southwest University of Science and Technology, Mianyang, China | <sup>3</sup>Science and Research Centre of Functional Nano-Ceramics, National University of Science and Technology "MISIS", Moscow, Russia | <sup>4</sup>Institute of General and Inorganic Chemistry of the National Academy of Sciences of Belarus, Minsk, Belarus | <sup>5</sup>State Key Laboratory of Solid Waste Resource Utilization and Energy Saving Building Materials, Beijing, China | <sup>6</sup>Institute of Chemistry, Saint Petersburg State University, St. Petersburg, Russia | <sup>7</sup>Research Laboratory of Scanning Probe Microscopy, Moscow Polytechnic University, Moscow, Russia | <sup>8</sup>Department of Materials Science and Engineering, University of Virginia, Charlottesville, Virginia, USA

**Correspondence:** Valentin Romanovski (rvd9ar@virginia.edu)

**Received:** 29 September 2024 | **Revised:** 16 October 2024 | **Accepted:** 6 November 2024

**Funding:** This work was supported by financial support of the Moscow Polytechnic University within the framework of the Kapitsa grant program.

**Keywords:** anhydrite cement | crystals | lime mud | processing technology | structure-guided method | synthetic anhydrite

## ABSTRACT

In the process of water treatment from surface water sources, lime mud as waste is formed. This waste contains CaO, Ca(OH)<sub>2</sub>, and CaCO<sub>3</sub>. The article proposes a comprehensive method for processing lime mud into high-strength anhydrite cement. The method involves the interaction of lime mud with waste sulfuric acid from the production of polymer fibers using a structure-controlled method in the (CaO·Ca(OH)<sub>2</sub>·CaCO<sub>3</sub>)—H<sub>2</sub>SO<sub>4</sub>—H<sub>2</sub>O system at a temperature of 40°C. X-ray diffraction analysis showed the presence of CaSO<sub>4</sub> and CaSO<sub>4</sub>·0.62H<sub>2</sub>O phases with a purity of 99.8%. The structure-controlled method makes it possible to control the formation and growth of calcium sulfate crystals of the required shape and size, due to which it is possible to obtain anhydrite cement with desired properties. Combined grinding of synthetic anhydrite with activator additives makes it possible to obtain anhydrite cement with a strength of up to 28.5 MPa.

## 1 | Introduction

The main problem of existing modern industrial production is the formation of various wastes at all technological stages. Recycling-generated waste is relevant and is part of the modern economy [1, 2]. However, most environmental projects are not profitable and are carried out only due to the positive environmental effect. A positive economic effect can be achieved either

by replacing expensive raw material components or by producing an expensive product [3–5], for example, building and construction materials [6, 7].

Water treatment processes also generate waste that requires disposal [8–10]. To coagulate water from surface water bodies, in the process of water treatment, iron and aluminum-containing coagulants are used. To increase the efficiency of coagulation

This is an open access article under the terms of the [Creative Commons Attribution](https://creativecommons.org/licenses/by/4.0/) License, which permits use, distribution and reproduction in any medium, provided the original work is properly cited.

© 2024 The Author(s). *Engineering Reports* published by John Wiley & Sons Ltd.

and carbon dioxide binding, additional lime is added. Thus, the precipitate that falls out during the coagulation process contains predominantly calcium carbonate and hydroxides of iron and aluminum. During the storage of lime (CaO), its “aging” occurs. Part of the lime is hydrated under the influence of atmospheric moisture, and carbon dioxide is also absorbed to form calcium carbonate.

Water treatment waste (precipitates from coagulation of natural waters and missing lime) due to the constancy of its composition and significant production volumes are a potential raw material. These wastes are generated during the preparation of water from surface sources at enterprises in various industries. The volume of their formation at an average enterprise (energy industry, radio electronics, etc.) amounts to up to 1000 tons per year.

A widely used method for using this waste, proposed in the literature, is thermal regeneration [11] to produce quicklime (CaO). Given the need to decompose calcium carbonate, the operating temperature of the process should be around 1000°C.

Waste of lime mud can be considered as a raw material for the production of synthetic gypsum [12, 13], despite the fact that gypsum itself is not used in construction and is a cheap raw material. Most of the gypsum used is natural. At the same time, the production of synthetic gypsum is also widespread, especially in countries where there are no natural deposits of it [14]. It should be noted that the use of commercial sulfuric acid to produce synthetic gypsum makes production economically ineffective. A solution in this situation may be the use of sulfuric acid waste or the production of expensive binding materials based on it [15–17]. The production of gypsum binders is traditionally carried out by autoclave processing of gypsum at elevated temperatures and pressure.

Another promising direction is the processing of lime mud into synthetic calcium sulfate anhydrite in one stage when interacting with sulfuric acid waste [16]. One of the key factors in this production method is the ability to control the structure of the resulting crystals [18–21]. By controlling the shape and size of the crystals, it is possible to obtain a material with improved characteristics compared to natural materials.

The objectives of the work were: (1) to obtain calcium sulfate anhydrite in one stage in the system  $(\text{CaO} \cdot \text{Ca}(\text{OH})_2 \cdot \text{CaCO}_3) - \text{H}_2\text{SO}_4 - \text{H}_2\text{O}$  at a temperature of 40°C, bypassing the stage of formation of calcium sulfate dihydrate with control of the structure of its crystals; (2) develop a waste-free, low-energy-intensive technology for processing lost lime into synthetic anhydrite; (3) conduct research on the influence of the amount and type of additives on the activation of the astringent properties of synthetic anhydrite during joint grinding.

## 2 | Materials and Methods

### 2.1 | Materials and Reagents

Waste lime mud was taken from the sludge storage facility of the city thermal power plant, formed during the process of

coagulation of water from the river. To form intergrowths of gypsum crystals, the flocculant Praestol 2515 was used with a dose of 0.2 wt% by weight of the initial carbonate raw material. To activate the astringent properties, the following additives were used: Portland cement grade PC500D0,  $\text{Ca}(\text{OH})_2$ , and  $\text{K}_2\text{SO}_4$ . The composition, purity, and suppliers of materials and reagents used are presented in the [Supporting Information file](#).

### 2.2 | Synthesis of Anhydrite

At the first stage, a suspension of lime mud was obtained at a ratio of S:L = 1:6. Next, the suspension was heated to 40°C and spent sulfuric acid with a concentration of 55 wt% was added at a feed rate of no more than 1 L of acid per 1 L of suspension with constant stirring at a stirrer speed of no more than 300 rpm. Next, the flocculant Praestol 2515 was dosed into the reactor in an amount of 0.2 wt% of the dry part of the suspension of the formed calcium sulfate dihydrate. After this, the suspension was sent for thickening for 60 min, which made it possible to enlarge the resulting calcium sulfate anhydrite crystals to particles > 80 μm in size. Next, the suspension of synthetic calcium sulfate was filtered, and the solid part was sent for drying at 90°C–95°C. The next stage in the preparation of the binder was the combined grinding of the resulting synthetic calcium sulfate with additives that activate astringent properties and produce anhydrite cement.

### 2.3 | Samples Characterization

The obtained samples of synthetic calcium sulfate anhydrite and the resulting binders based on it were analyzed for the following indicators: normal density measurements were performed according to standard [22]; measuring setting time using a Vicat apparatus; determination of the compressive strength of samples measuring 20 × 20 × 20 mm was measured on a universal testing machine “Instron 1195” [23].

Particle size distribution was determined using a Fritsch Particle Sizer Analysette 22 (Germany). The morphology and elemental composition of the surface of the samples were studied by samples of synthetic gypsum using scanning and transmission electron microscopy methods. The phase composition was determined using a D8 ADVANCE “Bruker” x-ray diffractometer (Germany). Thermogravimetric analysis (TGA) and differential scanning calorimetry (DSC) were carried out on a DTA NETZSCH STA 409 PC/PG device (Germany). A more detailed description of the methods used for analyzing the obtained samples is presented in the [Supporting Information file](#).

The article presents the average values of the measurements taken, indicating the standard deviation intervals of three parallel measurements.

### 2.4 | Biotesting of Mineral Filtrate

To assess the possibility of using mineral filtrate in agriculture as a fertilizer, its biotesting was carried out. Oilseed radish (*Raphanus sativus ssp. oleifera* Metzg.) was chosen for the experiment. Biotesting was done in November 2023. One hundred seeds were planted in two containers. Watering was carried out once a

day with a small amount of water to maintain the required soil moisture. One container was watered only with tap water, and the second container was watered with water, but on days 5, 7, 9, 11, and 13 it was watered with a filtrate solution instead of water. Oilseed radish was grown for 20 days. Temperature range 15°C–20°C. The results of seed germination were assessed according to GOST 33777-2016, GOST 12038-84, GOST 33061-2014, ISO 22030-2009 according to the following indicators: shoot length, main root length, wet weight, dry weight.

## 2.5 | Economic Feasibility

For the economic analysis the following criteria were calculated and considered: estimated capital and operational costs, annual net effect (ANE), simple payback period (SPP), net present value (NPV); internal rate of return (IRR), profitability index (IP), dynamic payback period (DPP). The detailed methodology is presented in the paper [3].

## 3 | Results and Discussion

### 3.1 | Characteristics of Synthetic Anhydrite

According to the XRD results presented in Figure 1 a, it is clear that the synthesized material in its composition is a mixture of  $\text{CaSO}_4$  with an Orthorhombic crystal lattice and  $Bmmb$  (63) space group and  $\text{CaSO}_4 \cdot 0.62\text{H}_2\text{O}$  with a Hexagonal crystal lattice and  $P3121$  (152) space group (Table 1). XRD shows a significant shift of the peaks of anhydrite obtained from lime mud to the left, relative to the peaks of thermal anhydrite obtained from natural gypsum. This shift of the peaks to the left indicates an increase in the interplanar distance. Thus, the shift in interplanar distances for the 020 plane of the crystal lattice is 3.5045 and 3.4517 Å, for the (012) plane—2.8551 and 2.8122 Å, for the (121) plane—2.8069 and 2.7619 Å, for the (220) plane—2.4766 and 2.4463 Å, and for the (202) plane—2.3315 and 2.3229 Å, respectively, for anhydrite from lime mud and thermal anhydrite. These displacements are

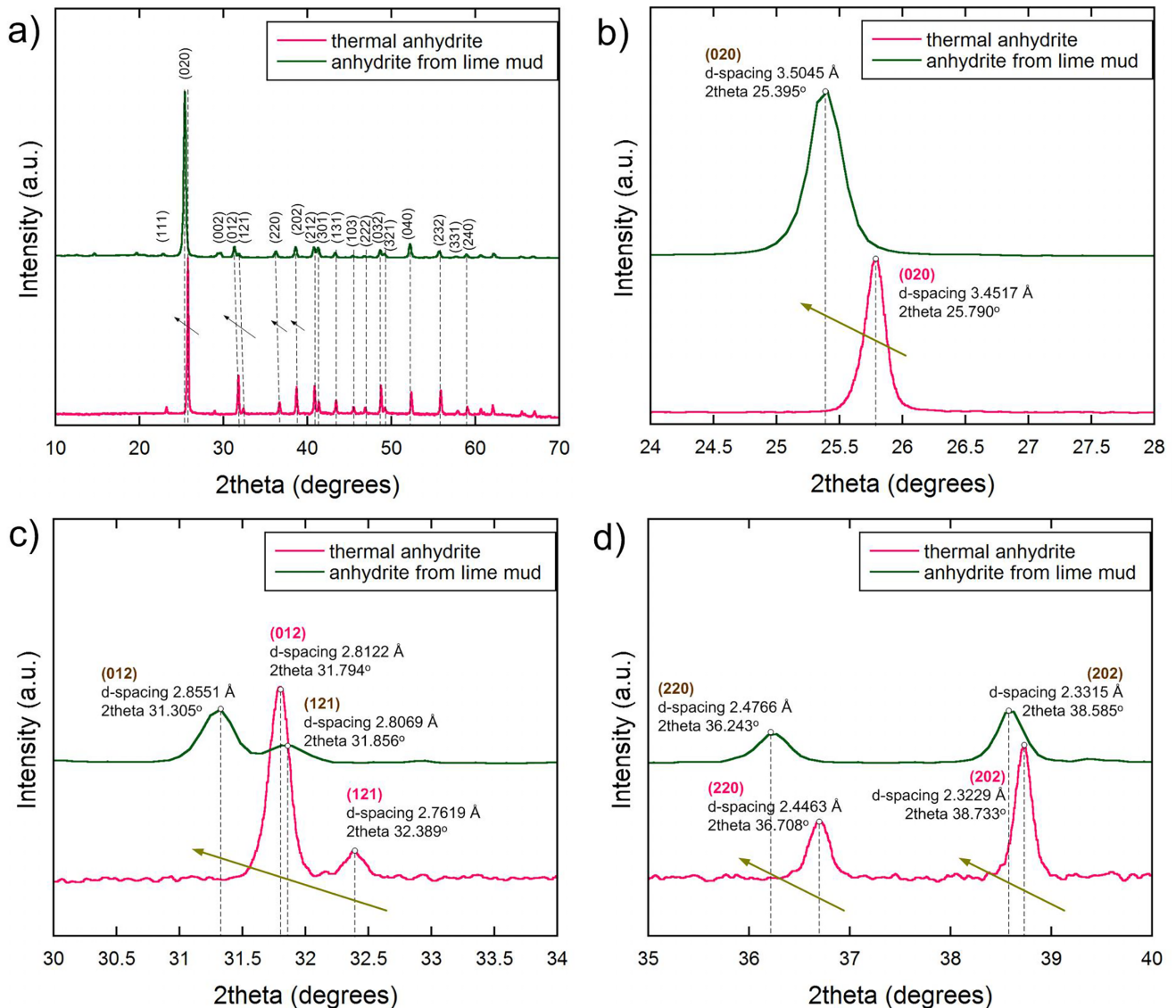


FIGURE 1 | Comparison of x-ray diffraction analysis of thermal anhydrite from natural gypsum and the resulting synthetic anhydrite from lime mud.

TABLE 1 | Comparison of crystal lattice parameters.

| Sample                  | Lattice parameters   |         |    |    |     |   |        |        |    |    |    |
|-------------------------|--|---------|----|----|-----|---|--------|--------|----|----|----|
|                         | CaSO <sub>4</sub> ·0.62H <sub>2</sub> O hexagonal, P3121 (152) |         |    |    |     | CaSO <sub>4</sub> orthorhombic, Bmmb (63) |        |        |    |    |    |
|                         | A  | c       | α  | β  | γ   | a   | b      | c      | α  | β  | γ  |
| Thermal anhydrite       |  |         |    | —  |     | 7.0803                                    | 7.1121 | 6.2577 | 90 | 90 | 90 |
| Anhydrite from lime mud | 13.9776  | 12.9536 | 90 | 90 | 120 | 7.5169                                    | 7.0704 | 6.3383 | 90 | 90 | 90 |

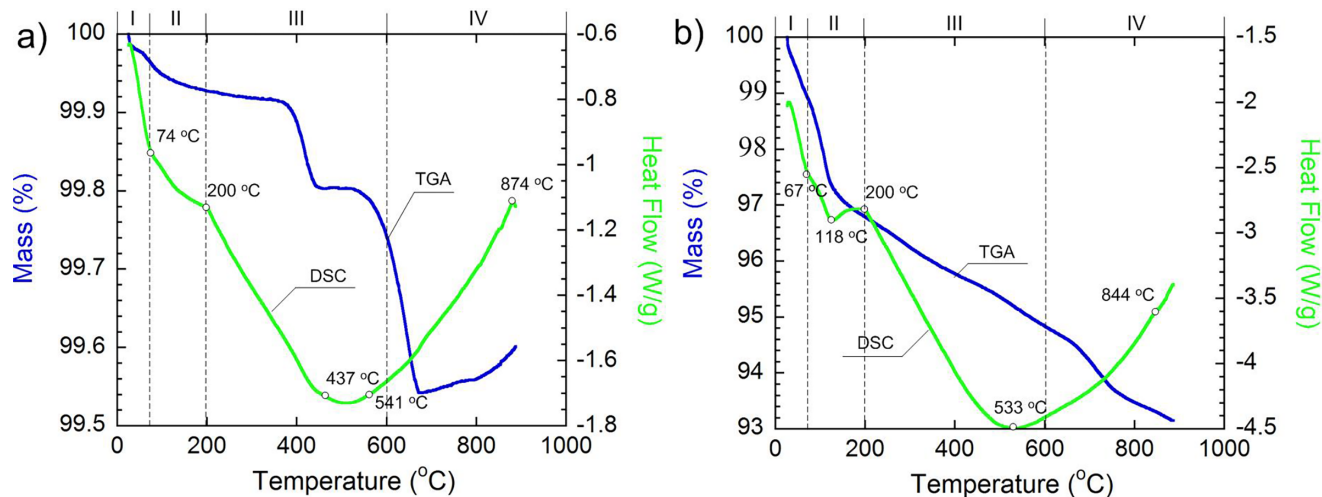


FIGURE 2 | DTA of thermal anhydrite from natural gypsum (a) and the resulting synthetic anhydrite from lime mud (b).

associated with defects in the crystal lattice of the synthesized anhydrite.

Data from differential thermal analysis (DTA) of the synthesized material, obtained by heating in the temperature range of 20°C–900°C with a temperature rise rate of 5°C/min (Figure 2 b), correlate with the results of DTA of thermally obtained anhydrite from natural gypsum at the firing temperature 700°C–900°C (Figure 2a).

As can be seen from Figure 2, the samples are similar in nature, but have differences both in the main effects and in the temperatures at which they occur. Thus, the first difference is observed in regions I and II: in thermally produced anhydrite, the process of removing physical moisture and dehydration occurs smoothly and begins at 74°C and ends at 200°C and is associated with a decrease in mass by 0.22 wt%. In turn, for synthetic anhydrite the process begins at 67°C and also ends at 200°C. The process of removing physical moisture occurs up to 118°C with a decrease in mass to 97.4 wt%. A significant difference of this sample is the presence of an effect in the range from 118°C to 200°C with a weight loss of 0.5 wt%. This is due to the presence of the CaSO<sub>4</sub>·0.62H<sub>2</sub>O phase. Data obtained using DTA allow us to establish that the sample contains 6.59 wt% CaSO<sub>4</sub>·0.62H<sub>2</sub>O, which causes this effect. The third region is caused by the phase transition of the dissolved form of anhydrite to the insoluble one. For thermal anhydrite, this region is located in the temperature range from 200°C to 541°C and is caused by a mass loss of 0.24 wt%. For synthetic anhydrite, this region lies in the

temperature range from 200°C to 600°C with a mass change of 4 wt%. These differences are due to differences in the nature of the origin of the materials, which shifts the temperature values. The higher weight loss of 3.76 wt% for synthetic anhydrite than for thermal anhydrite is associated with the removal of physical moisture from the crystals, which remained in the pores, cracks, and voids of the crystals. This is due to the process of its synthesis, since it was carried out in an aqueous environment and during the growth of crystals, the defects described above were formed, and water was thereby captured inside the crystal (Figure 3). In region IV, both for a sample of thermal and synthetic anhydrite, further heating of the material activates the formation of a small amount of CaO and the decomposition of relict calcium and magnesium carbonates. Based on the data obtained, as well as the results of elemental analysis (SEM-EDS), it follows that the purity of the obtained anhydrite is 99.8 wt%, with an admixture of 0.2 wt% magnesium sulfate.

As can be seen from the micrographs presented in Figure 4, the crystals of synthetic anhydrite have a prismatic or scaly shape and are overwhelmingly found in the form of intergrowths rather than single crystals. The data obtained using dispersion analysis presented in Figure 5 confirms, that in the controlled synthesis of synthetic anhydrite, crystal intergrowths are formed. As can be seen from Figure 4, 98.2% of the particles lie in the range of 345–600 μm.

It should be noted that the lime mud was stored in a sludge storage facility for more than a year. During this time, more

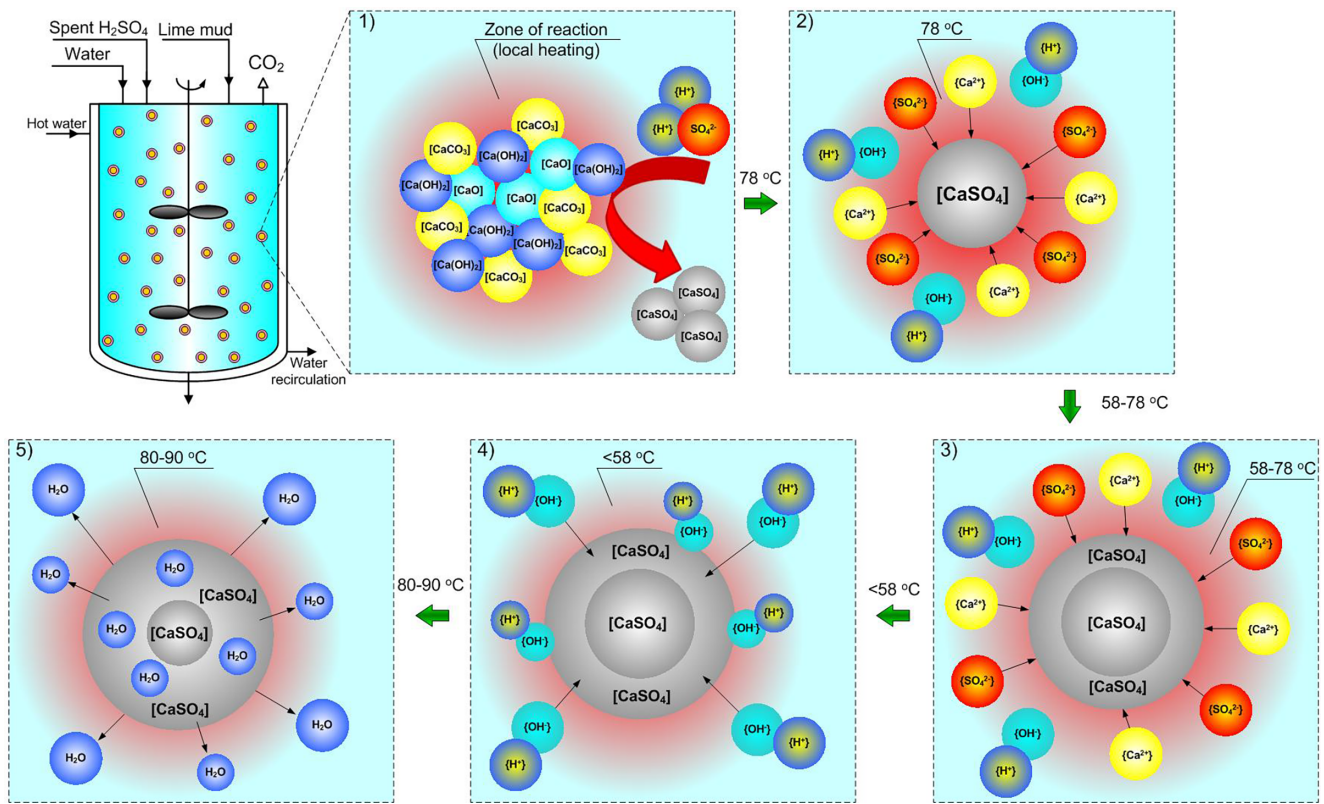


FIGURE 3 | Scheme of the formation of synthetic anhydrite from waste lime in the system  $(\text{CaO}\cdot\text{Ca}(\text{OH})_2\cdot\text{CaCO}_3)\text{--H}_2\text{SO}_4\text{--H}_2\text{O}$ .

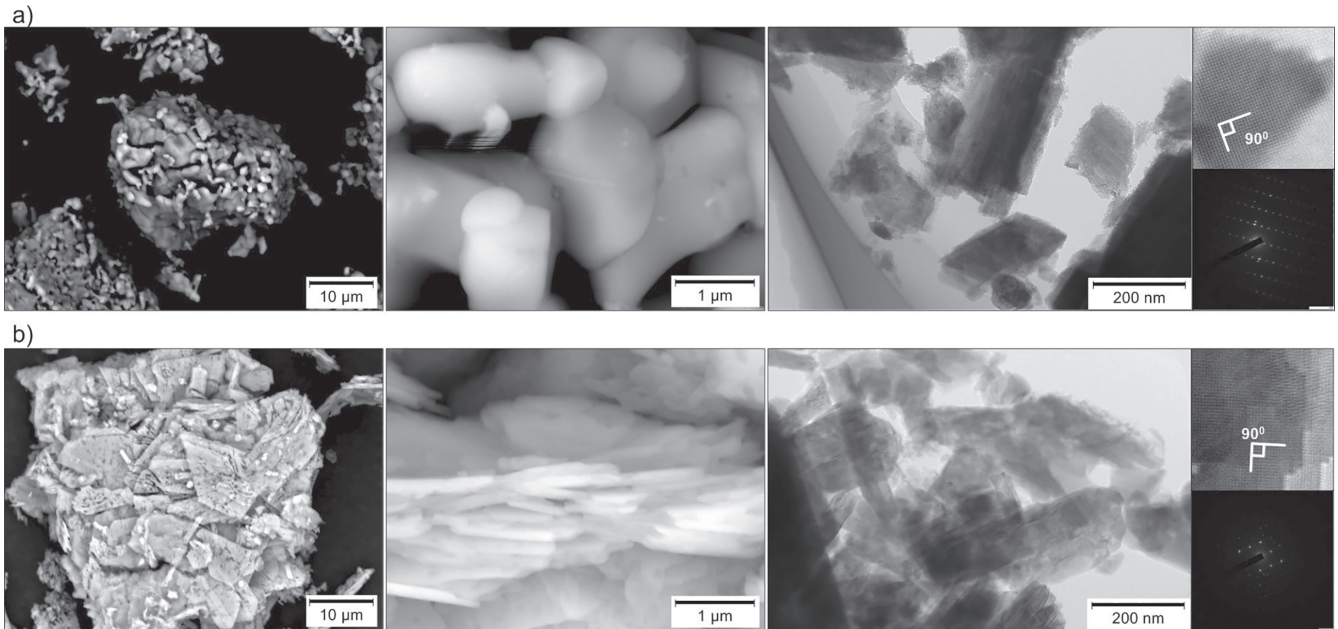
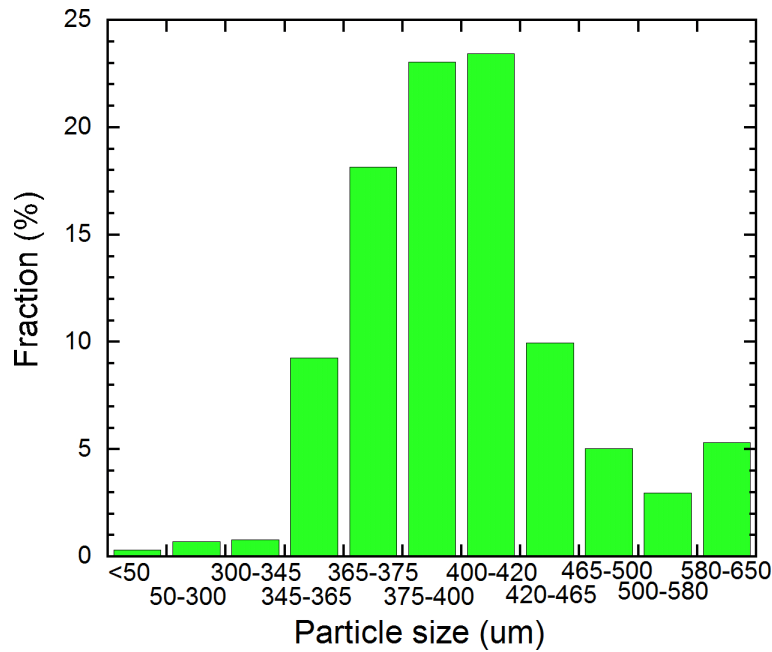


FIGURE 4 | SEM and TEM images of thermal from natural gypsum (a) and the resulting synthetic anhydrite from waste of lime mud (b).

CaO bound with water and carbon dioxide. Thus, we mean that, based on the composition of lime mud, this is the most pragmatic (complex) option for producing anhydrite in an aqueous environment in one stage. When setting up production and using the “younger” lime mud, it will contain a higher content of CaO, which will have a positive effect on the process due to the possibility of obtaining pure anhydrite.

### 3.2 | The Mechanism for Obtaining Anhydrite From Lime Mud

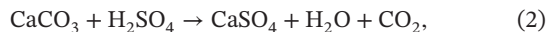
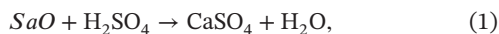
The synthesis of calcium sulfate anhydrite from lime mud can be represented as a scheme consisting of five stages, presented in Figure 3. The synthesis begins by mixing lime mud with water in a ratio of 1:6, after which a homogeneous suspension is obtained,



**FIGURE 5** | Synthetic anhydrite particle size distribution.

heated to 40°C with constant stirring at a stirrer speed of 300 rpm. Next, 53–55 wt% sulfuric acid is fed into the reactor at a flow rate of 1 L/L of suspension.

Stage 1: When sulfuric acid enters the reactor, the process of its dilution occurs with the release of additional heat, and the process of interaction with particles of missing lime begins with the formation of CaSO<sub>4</sub> crystals according to the reactions:



Based on these reactions, thermochemical calculations were carried out [15], which made it possible to prove the possibility of the formation of calcium sulfate anhydrite, rather than calcium sulfate dihydrate, due to local heating around the resulting particles to 78°C. Self-heating is caused by reactions (1) and (3), during which a significantly larger amount of heat is released than during the reaction proceeding according to equation (2).

Stage 2: At this stage, active growth (enlargement) of embryos occurs due to Ca<sup>2+</sup> and SO<sub>4</sub><sup>2-</sup> ions. Water particles do not cause the hydration process (do not bind) to the formed CaSO<sub>4</sub> crystals due to the elevated temperature (78°C) at the surface of the crystal.

Stage 3: At this stage, further growth of CaSO<sub>4</sub> crystals occurs and a gradual decrease in temperature at the surface of the growing crystal to 58°C. At this stage, an increase in the bulk of the crystal occurs, but at the same time, as at the previous stage, the hydration process is impossible, which was also proven by us earlier from the point of view of thermochemistry [16].

Stage 4: This stage is caused by a decrease in the temperature around the crystal below 58°C, which, from the point of view

of thermochemistry, causes the beginning of the CaSO<sub>4</sub> hydration process. Thus, at this stage, further crystal growth occurs with simultaneous surface hydration. As a result, a particle with a CaSO<sub>4</sub> core and a surface layer of CaSO<sub>4</sub>·2H<sub>2</sub>O is formed, and the process of H<sub>2</sub>O diffusion from the surface layer (“hydrated”) to the “anhydrous core” begins.

Stage 5: This stage is determined by the drying process of the resulting material at 80°C–90°C. At this stage, the process of evaporation of the remaining moisture occurs to prevent complete hydration. However, a hydrated layer is already present in the particle and this temperature is not enough to remove crystallization water, and increasing the temperature is impractical since a gypsum binder will be obtained with a compressive strength of 2–4 MPa [17]. Due to the presence of crystallization water, further diffusion of water molecules to the particle core occurs. Due to this, the presence of the CaSO<sub>4</sub>·0.62H<sub>2</sub>O phase is observed in the XRD results. The presence of this phase is also confirmed by the loss of mass shown in the DTA of the samples.

### 3.3 | Preparation of Anhydrite Binders

From our previous studies on the production of synthetic gypsum [17], it was found that the main properties of the gypsum binder obtained from this gypsum are influenced by the size of its particles. The larger the calcium sulfate dihydrate particles, the less water is needed (reduction in the water-gypsum ratio) to mix the gypsum binder to obtain normal density following GOST 23789-2018 [22]. By reducing the water-gypsum ratio, the wedging effect of water is reduced and the strength characteristics of the gypsum binder are increased. Since the synthesis of anhydrite was carried out in the same way as the synthesis of gypsum in the (CaO·Ca(OH)<sub>2</sub>·CaCO<sub>3</sub>)—H<sub>2</sub>SO<sub>4</sub>—H<sub>2</sub>O system, it was found that an increase in particle size has a positive effect on the properties of anhydrite cement obtained from synthetic anhydrite.

After the centrifugation step, an anhydrite cake is formed in the form of lump material. The next stage in the technology is the drying stage at a temperature of 80°C–90°C, which allows you to remove residual physical moisture after centrifugation. The established dependence of the mass loss of synthetic anhydrite on the drying time in an oven is presented in Figure 6.

As can be seen from the dependence presented in Figure 6, the optimal drying period lies in the range of 90–120 min. When drying for more than 120 min, no significant change in the mass of the sample is observed (the change occurs by only 0.1 wt%), and accordingly, this is an extra energy expenditure. If the drying

process takes less than 90 min, a significant amount of physical moisture will remain in the material, which will cause natural hydration of the anhydrite and, accordingly, a loss of strength characteristics.

The next technological operation after the drying process (the drying process in the laboratory was carried out in a drying cabinet) is the stage of grinding synthetic calcium sulfate anhydrite together with activator additives. We conducted research to study the grinding time to obtain anhydrite cement that meets the standard for residue on sieve No. 02. Figure 7 shows the effect of

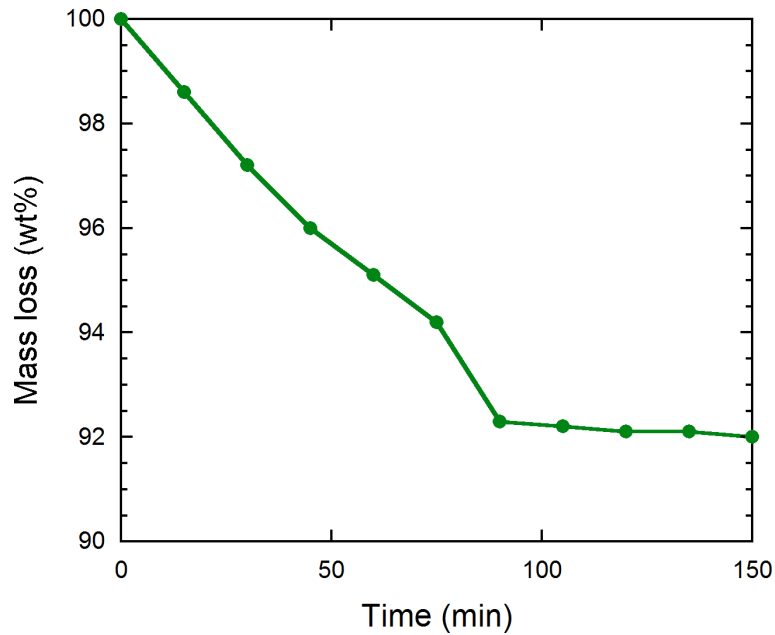


FIGURE 6 | Dependence of mass loss of synthetic anhydrite on drying time at constant temperature.

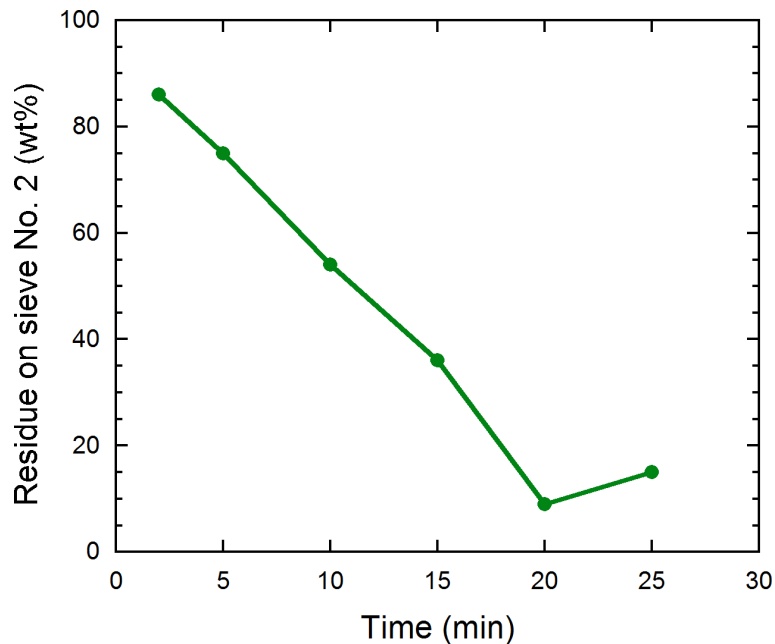


FIGURE 7 | Effect of grinding time on the grinding fineness of anhydrite cement.

grinding time on obtaining the final product with the required fraction.

From Figure 7 it can be seen that the optimal time is grinding for 20 min since the residue on sieve No. 02 is 9 wt%, which meets the requirements of the standard (EN 13279-2:2014 [24]) for gypsum binders. Grinding for more than 20 min leads to an increase in the residue on sieve No. 02 from 9 to 15 wt%. This is due to the agglomeration process, that is, the resulting small particles stick together to form secondary agglomerates. In this regard, grinding for more than 20 min will only lead to additional energy costs. Grinding for less than 20 min is not effective due to the large amount of material remaining on sieve No. 02, as can be seen from Figure 4 (with 15 min of grinding, the residue on the sieve is 36 wt%, and with a shorter grinding time, the residue on the sieve is more than 40 wt%).

The process of grinding synthetic anhydrite is carried out together with activator additives. This is because synthetic anhydrite, like thermally produced calcium sulfate anhydrite, does not exhibit astringent properties on a sufficient scale and the use of additives is necessary to activate them. The following materials were selected as additives: Portland cement brand PC500D0, potassium sulfate, and calcium hydroxide. However, using these additives separately does not give the desired result. Based on this, studies were carried out to establish the composition of the complex additive with the optimal content of the amount of each component in the mixture. To accurately determine the compressive strength, the amount of water used for mixing was selected to control the spread of the dough, in accordance with the standard. The research results are presented in Table 2.

The obtained values of the anhydrite water ratio are close to the values for anhydrite [25], obtained traditionally by firing at 700°C–900°C, which indicates that the material obtained using the developed technology is a promising analog.

Following the standard (GOST 23789-2018) [22], to fully describe the properties of the resulting materials, studies were carried out to determine the setting time using a Vicat device, the results of which are presented in Table 3.

As can be seen from the data presented in Table 2, the setting time for composition No. 10, which showed maximum compressive strength, the setting time is: beginning—40 min, end—12 h, which corresponds to the requirements of the standard.

As can be seen from the experimental data obtained, sample No. 10 has the best strength properties, in which the following additives were used to activate the binding properties: PC500D0–2.5 wt% and K<sub>2</sub>SO<sub>4</sub>–1.0 wt%. For a comparative assessment, a sample was obtained based on synthetic anhydrite obtained at 25°C and the additions of PC500D0–2.5 wt% and K<sub>2</sub>SO<sub>4</sub>–1.0 wt%. Comparative characteristics of the samples are presented in Table 4.

As can be seen from the results presented in Table 3, anhydrite cements obtained from different synthetic raw materials have different characteristics with the same high content of the main substance. And to activate astringent properties, it is necessary to use various activator additives with different contents [26, 27].

According to standards (e.g., EN 13279–2:2014), the compressive strength for anhydrite cement is usually a minimum of

TABLE 2 | Ultimate compressive strength of anhydrite cement samples aged 28 days.

| Sample | Additive, wt% |                                |                     | W/A   | Ultimate compressive strength, MPa |
|--------|---------------|--------------------------------|---------------------|-------|------------------------------------|
|        | PC500D0       | K <sub>2</sub> SO <sub>4</sub> | Ca(OH) <sub>2</sub> |       |                                    |
| 1      | 0             | 0                              | 0                   | 0.250 | 0                                  |
| 2      | 0             | 1.0                            | 0.1                 | 0.260 | 17.1 ± 1.36                        |
| 3      | 0             | 1.0                            | 0.2                 | 0.245 | 20.6 ± 0.63                        |
| 4      | 0             | 1.0                            | 0.3                 | 0.240 | 25.4 ± 1.38                        |
| 5      | 0             | 1.0                            | 0.4                 | 0.230 | 23.7 ± 1.10                        |
| 6      | 0.5           | 1.0                            | 0                   | 0.230 | 12.0 ± 0.36                        |
| 7      | 1.0           | 1.0                            | 0                   | 0.235 | 22.4 ± 0.72                        |
| 8      | 1.5           | 1.0                            | 0                   | 0.235 | 24.6 ± 0.82                        |
| 9      | 2.0           | 1.0                            | 0                   | 0.240 | 26.1 ± 0.66                        |
| 10     | 2.5           | 1.0                            | 0                   | 0.250 | 28.4 ± 1.12                        |
| 11     | 2.5           | 0.5                            | 0                   | 0.245 | 20.9 ± 0.61                        |
| 12     | 2.5           | 1.5                            | 0                   | 0.240 | 25.2 ± 0.92                        |
| 13     | 2.5           | 2.0                            | 0                   | 0.235 | 23.2 ± 0.46                        |
| 14     | 3.0           | 2.0                            | 0                   | 0.235 | 21.7 ± 0.54                        |
| 15     | 3.5           | 2.0                            | 0                   | 0.235 | 20.9 ± 1.08                        |
| 16     | 4.0           | 2.0                            | 0                   | 0.235 | 19.4 ± 0.96                        |
| 17     | 4.5           | 2.0                            | 0                   | 0.240 | 18.7 ± 0.38                        |
| 18     | 5.0           | 2.0                            | 0                   | 0.240 | 17.9 ± 1.21                        |

**TABLE 3** | Setting time for anhydrite cement samples.

| Sample | Setting time       |            |
|--------|--------------------|------------|
|        | Beginning, minutes | End, hours |
| 1      | —                  | —          |
| 2      | 65                 | 19.0       |
| 3      | 55                 | 15.5       |
| 4      | 45                 | 13.0       |
| 5      | 48                 | 14.0       |
| 6      | 85                 | 22.0       |
| 7      | 76                 | 19.5       |
| 8      | 64                 | 16.0       |
| 9      | 52                 | 14.5       |
| 10     | 40                 | 12.0       |
| 11     | 44                 | 12.5       |
| 12     | 47                 | 13.0       |
| 13     | 50                 | 13.5       |
| 14     | 49                 | 13.5       |
| 15     | 49                 | 13.5       |
| 16     | 47                 | 13.0       |
| 17     | 46                 | 13.0       |
| 18     | 45                 | 13.0       |

**TABLE 4** | Comparative characteristics of anhydrite cements obtained from calcium sulfate anhydrite synthesized at different temperatures.

| Parameters                      | Anhydrite cement obtained from     |                               |
|---------------------------------|------------------------------------|-------------------------------|
|                                 | Anhydrite synthesized at 25°C [25] | Anhydrite synthesized at 40°C |
| Setting time, beginning         | 2 h                                | 40 min                        |
| Setting time, end               | 20 h                               | 12 h                          |
| Water anhydrite (W/A) ratio     | 0.26                               | 0.25                          |
| Compressive strength at 28 days | 3.8 MIIa                           | 28.4 MIIa                     |

6–10 MPa, depending on the cement class (e.g., classes A5, A10). In the obtained samples, the maximum strength (28.4 MPa) significantly exceeds this value, which indicates high strength of the obtained material. For the setting time, according to EN standards, the onset of setting of anhydrite cement should be no earlier than 30 min, and the end—no later than 24 h. In Table 3, the setting start time varies from 40 to 85 min, which is in line with the standard. The end of setting is also within the norm, with a maximum time of 22 h. The strength results in Table 2 show that the obtained anhydrite cement exceeds the minimum strength requirements of EN standards. In addition, the setting start and end times from Table 3 fully comply with the requirements.

### 3.4 | The Technology for Producing Anhydrite Cement From Lime Mud

The complex technology for processing lime mud into synthetic anhydrite with its subsequent conversion into anhydrite cement is presented in Figure 8. At the first stage, a suspension of insufficient lime is prepared with the ratio S: L = 1: 6 in reactor 6. Lime mud is supplied to the reactor from the warehouse by an electric hoist (1) through the supply hopper (3). To prepare the suspension, water is then supplied or the resulting filtrate can be used at the centrifugation stage. At room temperature and constant stirring at a speed of 300 rpm in the reactor (6), sulfuric acid (53–55 wt%) is supplied from the supply tank (4) through the flow meter (5). To achieve greater environmental and economic efficiency in the technology, it can be used spent sulfuric acid at a rate of 0.65–1 L of acid per 1 L of suspension.

After all the acid necessary for the process (calculated from stoichiometric reactions) has been supplied to the reactor (6), an aggregating component is supplied to it—a Praestol flocculant in an amount of 0.2 wt% of the theoretically calculated amount of the resulting synthetic anhydrite calcium sulfate. After supplying the flocculant to the reactor (6), the stage of thickening the resulting calcium sulfate anhydrite suspension begins, which is carried out with constant stirring at a stirrer speed of 100–150 rpm for 60 min. The condensation stage is completed after the gas phase (a mixture of CO<sub>2</sub> and H<sub>2</sub>O) has ceased to separate from the resulting suspension. The next step is the supply of the suspension from the reactor (6) to the thickener (7), where the aging process of the suspension is carried out for 90 min at room temperature, which is carried out to further enlarge the particles of synthetic anhydrite due to their growth and aggregation. Next, the suspension from the thickener (7) is sent to a centrifuge (8) to separate the solid phase—synthetic anhydrite with moisture (8–10 wt%) and the liquid phase—filtrate. The solid phase (synthetic calcium sulfate anhydrite) from the centrifuge (8) along a belt conveyor (10) is fed into the supply hopper (11), after which it is fed into the dryer (12) to remove residual physical moisture at a temperature of 80°C–90°C for 90–120 min. The dried material is supplied for co-grinding with activator additives in a mill (13) where it is crushed to the required fraction in accordance with GOST and then sent for packaging. The optimal parameters for anhydrite production are presented in Table 5.

The technological scheme in Figure 8 was designed with scalability in mind, as each stage relies on well-established industrial equipment (e.g., reactors, centrifuges, mills) that can be scaled up without significant changes to process parameters. The low operating temperature of 40°C, compared to conventional methods requiring 700°C–900°C, reduces energy consumption, making the process more feasible and sustainable for industrial application. Additionally, the use of industrial by-products like lime mud and spent sulfuric acid ensures a consistent supply of raw materials, while the closed-loop system for filtrate recycling minimizes waste and improves cost-effectiveness at larger scales. Given these factors, the process is promising for industrial scalability, though further pilot-scale studies are recommended to optimize performance under different industrial conditions.

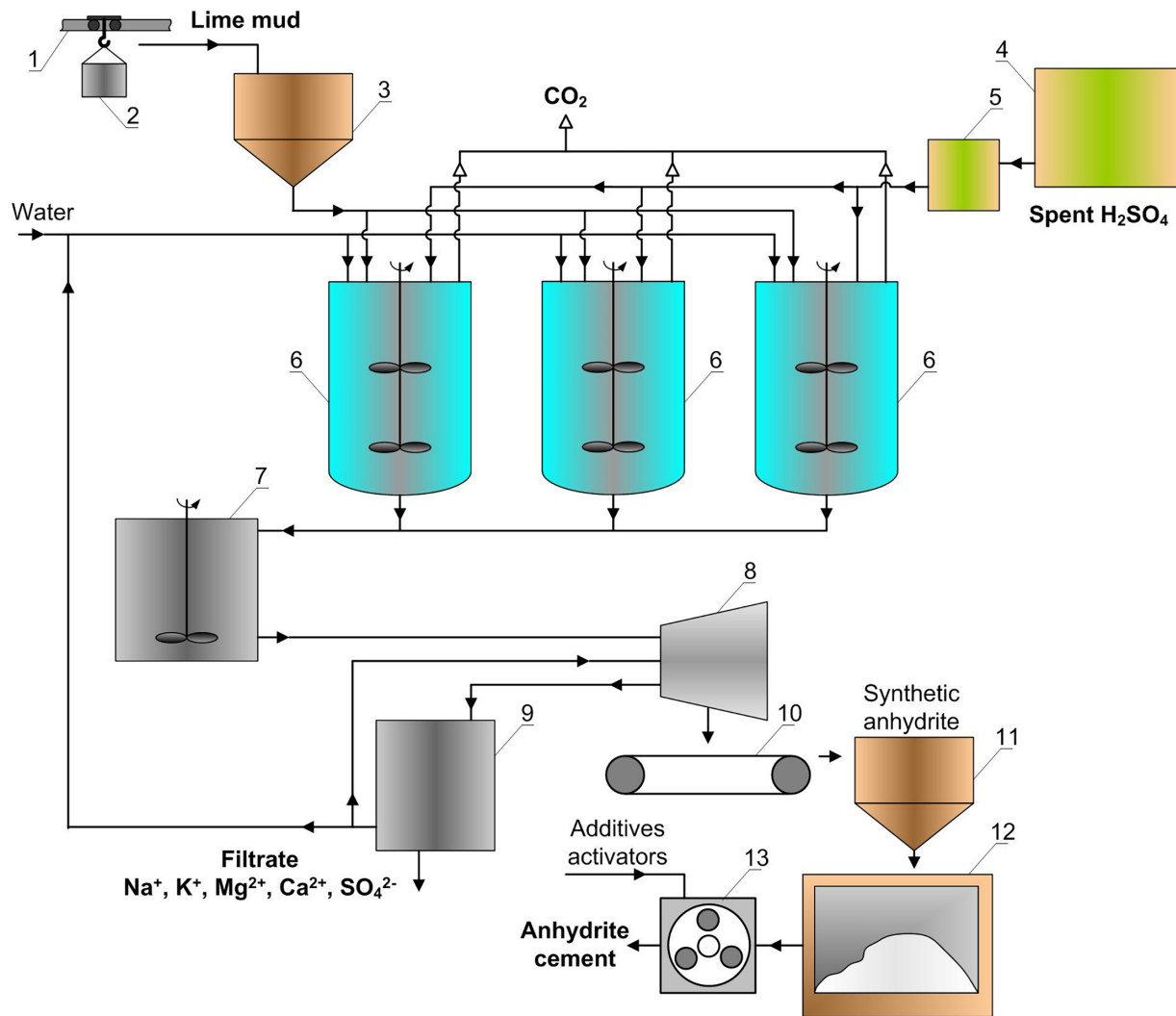


**FIGURE 8** | Basic technological scheme for producing anhydrite cement from lime mud: 1—electric hoist; 2—big bag; 3—bunker; 4—sulfuric acid tank; 5—flow meter; 6—reactor; 7—thickener; 8—centrifuge; 9—thickener; 10—belt conveyor; 11—supply hopper; 12—dryer; 13—mill.

The prospects for further research using machine learning methods include the ability to more accurately predict anhydrite cement properties, such as strength and setting time, based on different combinations of raw materials and process parameters [28–32]. This will allow for the optimization of formulations and synthesis conditions, leading to the creation of materials with improved properties at minimal cost. In addition, machine learning can reveal hidden dependencies and trends that are difficult to detect using traditional analysis methods.

### 3.5 | Direction of Use of Filtrate

The liquid phase (filtrate) from the centrifuge (8) is sent to the collection tank (9). From it, the filtrate can be sent to prepare a suspension of insufficient lime, but this option is possible no more than three times since dissolved Na, Mg, K compounds accumulate in the filtrate, which, at elevated concentrations, negatively affect the growth of synthetic anhydrite crystals. The second option for using the filtrate is its use as a microfertilizer for watering plants, due to the  $\text{Na}^+$ ,  $\text{Mg}^{2+}$ ,  $\text{K}^+$ ,  $\text{SO}_4^{2-}$  ions dissolved in it.

In a box in which only water was used for irrigation, the germination efficiency was 83%, and in a box in which filtrate was additionally used for irrigation—84% what is in a good agreement with average germination efficiency [33]. When using filtrate for irrigation, the height of almost half of the sprouts increased to 14% compared to the test irrigation with water, while the length of the main root for both samples has almost the same values. When performing a bioindication experiment for a longer period of time and increasing the dose of applied fertilizer, better results should be expected.

The presence of sodium and sulfur in the fertilizer makes it effective for beets and cruciferous plants that respond positively to these elements. The sulfur content significantly increases the percentage of gluten and healthy proteins in wheat and rye [34–36]. The product can be applied to the soil not only in early spring, but also in autumn, since small particles of fertilizer are perfectly fixed in the soil and are not washed out. The composition of the resulting product also contains magnesium ions. A lack of magnesium in the soil and fertilizing leads to a deterioration in photosynthesis, because on its basis the molecular structure of chlorophyll is formed [34–36]. The fertilizer

**TABLE 5** | Optimal values of technological parameters.

| Parameter  | Value                             |
|--|-----------------------------------|
| The S: L ratio when preparing the lime mud suspension            | 1: 6                              |
| The temperature of the lime mud suspension                       | 40°C                              |
| Mixer rotation speed   | 300 rpm                           |
| H <sub>2</sub> SO <sub>4</sub> concentration                     | 53–55 wt%                         |
| H <sub>2</sub> SO <sub>4</sub> consumption                       | 1 L of acid per 1 L of suspension |
| Amount of Praestol 2515 based on the amount of final solid phase | 0.2 wt%                           |
| Thickening period  | 60 min                            |
| Mixer rotation speed during the thickening process               | 100–150 rpm                       |
| Aging period   | 90 min                            |
| Drying temperature   | 85°C–90°C                         |
| Drying period  | 90–100 min                        |
| Grinding time  | 20 min                            |

obtained from the filtrate should ensure enhanced production of sugar and vitamin C. At the same time, thanks to magnesium, the content of essential oil, fats and other substances valuable for the human diet increases in the leaves and fruits [34–36].

### 3.6 | Economic Feasibility

The lime mud recycling process involves the use of 505 tons of lime mud waste and 1068 tons of spent acid, while energy consumption is 43,000 kW·h. 2020 tons of water are used as additional raw materials. The processing results in 790.7 tons of anhydrite and 14.05 tons of sulfate fertilizer. At the same time, CO<sub>2</sub> emissions are 171.16 tons. The current production costs are \$ 44,200, but the total annual economic effect reaches \$ 83,800. The simple payback period is 0.7 years, and the dynamic payback period is 0.9 years, which indicates high economic efficiency of the project. The net present value is estimated at \$ 459,300, the internal rate of return is 0.63, and the profitability index is 9.26, which confirms the high profitability and attractiveness of investments in this recycling process.

## 4 | Conclusion

Lime mud is a promising raw material for the production of synthetic calcium sulfate anhydrite with a purity of up to 99.8 wt%. The results obtained using XRD and DTA confirm that synthetic anhydrite is identical in its characteristics to anhydrite obtained using traditional technologies by firing at 700°C–900°C.

Anhydrite cement obtained from synthetic calcium sulfate anhydrite in its pure form does not have astringent properties. To activate the astringent properties, it is necessary to use activator additives (a mixture of PC500D0, K<sub>2</sub>SO<sub>4</sub>, Ca(OH)<sub>2</sub>), which make

it possible to activate the astringent properties and obtain a material with compressive strength at the age of 28 days of more than 28 MPa, and impart other properties (setting time, water anhydrite ratio) values in accordance with the standard.

The use of the filtrate formed at the stage of centrifugation of a synthetic anhydrite suspension as a microfertilizer is possible due to the presence of dissolved salts in it, which make it possible to increase the mass of the root system and increase the dry mass of the plant.

Low-energy complex technology for processing insufficient lime into anhydrite cement is a promising analogue to traditional technologies for producing anhydrite cement with significantly lower material costs—the simplicity of the technological scheme, as well as energy costs due to the main synthesis temperature: synthetic anhydrite at 40°C, thermal anhydrite at 700°C–900°C. The use of filtrate makes it possible to obtain an additional economic effect, and also due to its use allows us to call the developed technology waste-free (closed-cycle technology).

### Author Contributions

**Maksim Kamarou:** methodology, validation, investigation, formal analysis, data curation, writing – original draft. **Hongbin Tan:** formal analysis, data curation. **Dmitry Moskovskikh:** investigation, formal analysis, data curation. **Natallia Kulinich:** investigation, formal analysis, data curation. **Xiaoling Ma:** formal analysis, data curation. **Feihua Yang:** formal analysis, data curation. **Evgenii Beletskii:** investigation, formal analysis, data curation. **Elena Alekseeva:** formal analysis, data curation. **Sergey Yudin:** investigation. **Valentin Romanovski:** conceptualization, methodology, data curation, formal analysis, supervision, validation, investigation, visualization, writing – original draft, writing – review and editing.

### Ethics Statement

The authors have nothing to report.

### Consent

No written consent has been obtained from the patients as there is no patient identifiable data included.

### Conflicts of Interest

The authors declare no conflicts of interest.

### Data Availability Statement

All data, models, and code generated or used during the study appear in the submitted article.

### References

1. H. Zhou, D. Zhang, Y. Jiang, et al., “Recovery of Carbon From Spent Carbon Cathode by Alkaline and Acid Leaching and Thermal Treatment and Exploration of Its Application in Lithium-Ion Batteries,” *Environmental Science and Pollution Research* 30, no. 53 (2023): 114327–114335.
2. V. Zalyhina, V. Cheprasova, and V. Romanovski, “Pigments From Spent Chloride-Ammonium Zinc Plating Electrolytes,” *Journal of Chemical Technology and Biotechnology* 96, no. 10 (2021): 2767–2774, <https://doi.org/10.1002/jctb.6822>.

3. A. Hurynovich, M. Kwietniewski, and V. Romanovski, "Evaluation of the Possibility of Utilization of Sewage Sludge From Wastewater Treatment Plant – Case Study," *Desalination and Water Treatment* 227 (2021): 16–25, <https://doi.org/10.5004/dwt.2021.27199>.
4. A. Smorokov, A. Kantaev, D. Bryankin, A. Miklashevich, M. Kamarou, and V. Romanovski, "Low-Temperature Method for Desilicization of Polymetallic Slags by Ammonium Bifluoride Solution," *Environmental Science and Pollution Research* 30, no. 5 (2023): 30271–30280, <https://doi.org/10.1007/s11356-022-24230-y>.
5. I. Matsukevich, N. Kulinich, and V. Romanovski, "Direct Reduced Iron and Zinc Recovery From Electric Arc Furnace Dust," *Journal of Chemical Technology and Biotechnology* 97, no. 11 (2022): 3091–3099, <https://doi.org/10.1002/jctb.7205>.
6. M. Y. Abdulwahid, A. A. Akinwande, M. Kamarou, V. Romanovski, and I. A. Al-Qasem, "The Production of Environmentally Friendly Building Materials out of Recycling Walnut Shell Waste: A Brief Review," *Biomass Convers Biorefin* 14 (2023): 24963–24972.
7. V. N. Martsul, O. S. Zalygina, L. A. Shibeka, A. V. Likhacheva, and V. I. Romanovski, "Some Applications of Galvanic Manufacture Waste. Proceedings of BSTU," *Chemistry and Technology of Inorganic Substances* 3 (2012): 66–70.
8. V. I. Ramanouski and N. A. Andreeva, "Purification of Washing Waters of Iron Removal Stations. Proceedings of BSTU," *Chemistry and Technology of Inorganic Substances* 3 (2012): 62–65.
9. V. Yushchenko, E. Velyugo, and V. Romanovski, "Development of a New Design of Deironing Granulated Filter for Joint Removal of Iron and Ammonium Nitrogen From Underground Water," *Environmental Technology* 1-8 (2023): 2735–2742, <https://doi.org/10.1080/09593330.2023.2185820>.
10. V. Yushchenko, E. Velyugo, and V. Romanovski, "Influence of Ammonium Nitrogen on the Treatment Efficiency of Underground Water at Iron Removal Stations," *Groundwater for Sustainable Development* 22 (2023): 100943, <https://doi.org/10.1016/j.gsd.2023.100943>.
11. J. G. Li, L. H. Zhang, and F. Duan, "Effect of the Dried and Hydrothermal Sludge Combustion on Calcium Carbonate Decomposition in a Simulated Regeneration Reactor of Calcium Looping," *Energy & Fuels* 34, no. 4 (2020): 4745–4753.
12. M. Kamarou, M. Kuzmenkov, N. Korob, W. Kwapinski, and V. Romanovski, "Structurally Controlled Synthesis of Calcium Sulphate Dihydrate From Industrial Wastes of Spent Sulphuric Acid and Limestone," *Environmental Technology and Innovation* 17 (2020): 100582, <https://doi.org/10.1016/j.eti.2019.100582>.
13. M. Kamarou, N. Korob, and V. Romanovski, "Structurally Controlled Synthesis of Synthetic Gypsum Derived From Industrial Wastes: Sustainable Approach," *Journal of Chemical Technology & Biotechnology* 96, no. 11 (2021): 3134–3141, <https://doi.org/10.1002/jctb.6865>.
14. C. Wang, X. Ma, W. Zhong, et al., "Preparation of Calcium Sulfate From Recycled Red Gypsum to Neutralize Acidic Wastewater and Application of High Silica Residue," *Journal of Material Cycles and Waste Management* 1-8 (2024): 1588–1595, <https://doi.org/10.1007/s10163-024-01914-w>.
15. M. Kamarou, N. Korob, W. Kwapinski, and V. Romanovski, "High-Quality Gypsum Binders Based on Synthetic Calcium Sulfate Dihydrate Produced From Industrial Waste," *Journal of Industrial and Engineering Chemistry* 100 (2021): 324–332, <https://doi.org/10.1016/j.jiec.2021.05.006>.
16. V. Romanovski, A. Klyndyuk, and M. Kamarou, "Green Approach for Low-Energy Direct Synthesis of Anhydrite From Industrial Wastes of Lime Mud and Spent Sulfuric Acid," *Journal of Environmental Chemical Engineering* 9, no. 6 (2021): 106711, <https://doi.org/10.1016/j.jece.2021.106711>.
17. V. Romanovski, L. Zhang, X. Su, A. Smorokov, and M. Kamarou, "Gypsum and High Quality Binders Derived From Water Treatment Sediments and Spent Sulfuric Acid: Chemical Engineering and Environmental Aspects," *Chemical Engineering Research and Design* 184 (2022): 224–232, <https://doi.org/10.1016/j.cherd.2022.06.008>.
18. F. R. Massaro, M. Rubbo, and D. Aquilano, "Theoretical Equilibrium Morphology of Gypsum (CaSO<sub>4</sub>·2H<sub>2</sub>O). A Syncretic Strategy to Calculate the Morphology of Crystals," *Crystal Growth & Design* 10, no. 7 (2010): 2870–2878.
19. M. Kamalipour, S. A. M. Dehghani, A. Naseri, and S. Abbasi, "Role of Agitation and Temperature on Calcium Sulfate Crystallization in Water Injection Process," *Journal of Petroleum Science and Engineering* 151 (2017): 362–372.
20. P. G. Klepetsanis, E. Dalas, and P. G. Koutsoukos, "Role of Temperature in the Spontaneous Precipitation of Calcium Sulfate Dehydrate," *Langmuir* 15, no. 4 (1999): 1534–1540.
21. M. H. H. Mahmoud, M. M. Rashad, I. A. Ibrahim, and E. A. Abdel-Aal, "Crystal Modification of Calcium Sulfate Dihydrate in the Presence of Some Surface-Active Agents," *Journal of Colloid and Interface Science* 270, no. 1 (2004): 99–105.
22. Gypsum Binders, *Test Methods: GOST 23789-2018. Enter 05/01/2019* (Moscow: Standardinform, 2018), 17.
23. Metals, *Tensile Test Methods: GOST 1497-84. Enter 01/01/86* (Moscow: Standards Publishing House, 1984), 26.
24. EN, B. 13279-2:2014 *Gypsum Binders and Gypsum Plasters. Test methods* (Brussels: European Committee for Standardization, 2014), 23.
25. M. Singh and M. Garg, "Making of Anhydrite Cement From Waste Gypsum," *Cement and Concrete Research* 30, no. 4 (2000): 571–577, [https://doi.org/10.1016/S0008-8846\(00\)00209-X](https://doi.org/10.1016/S0008-8846(00)00209-X).
26. M. Kamarou, D. Moskovskikh, H. L. Chan, et al., "Low Energy Synthesis of Anhydrite Cement From Waste Lime Mud," *Journal of Chemical Technology and Biotechnology* 98 (2023): 789–796, <https://doi.org/10.1002/JCTB.7284>.
27. M. Kamarou, D. Moskovskikh, K. Kuskov, et al., "High-Strength Gypsum Binder With Improved Water Resistance Coefficient Derived From Industrial Wastes," *Waste Management & Research* (2024), <https://doi.org/10.1177/0734242X241240042>.
28. L. Ma, Y. Ghorbani, C. B. Kongar-Syuryun, et al., "Dynamics of Backfill Compressive Strength Obtained From Enrichment Tails for the Circular Waste Management," *Resources, Conservation & Recycling Advances* 23 (2024): 200224, <https://doi.org/10.1016/j.rcradv.2024.200224>.
29. V. S. Brigida, V. I. Golik, and B. V. Dzeranov, "Modeling of Coalmine Methane Flows to Estimate the Spacing of Primary Roof Breaks," *Mining* 2, no. 4 (2022): 809–821, <https://doi.org/10.3390/mining2040045>.
30. I. Viktorov and R. Gibadullin, "The Principles of Building a Machine-Learning-Based Service for Converting Sequential Code Into Parallel Code," in *E3S Web of Conferences*, vol. 431 (London, UK: EDP Sciences, 2023), 05012.
31. E. Kozlov and R. Gibadullin, "Prerequisites for Developing the Computer Vision System for Drowning Detection," in *E3S Web of Conferences*, vol. 474 (London, UK: EDP Sciences, 2024), 02031.
32. M. Nuriev and M. Lapteva, "Facilitating Efficient Energy Distribution and Storage: The Role of Data Consistency Technologies in Azure Cosmos DB," in *E3S Web of Conferences*, vol. 541 (London, UK: EDP Sciences, 2024), 02003.
33. V. Romanovski, S. Roslyakov, G. Trusov, et al., "Synthesis and Effect of CoCuFeNi High Entropy Alloy Nanoparticles on Seed Germination, Plant Growth, and Microorganisms Inactivation Activity," *Environmental Science and Pollution Research* 30, no. 9 (2023): 23363–23371.
34. V. Romanovski and R. Periakaruppan, "Why Metal Oxide Nanoparticles Are Superior to Other Nanomaterials for Agricultural Application?,"

in *Nanometal Oxides in Horticulture and Agronomy* (Cambridge, MA: Academic Press, 2023), 7–18, <https://doi.org/10.1016/B978-0-323-91809-1.0014-7>.

35. V. Romanovski, I. Matsukevich, E. Romanovskaia, and R. Periakaruppan, “Nano metal oxide as nanosensors in agriculture and environment,” in *Nanometal Oxides in Horticulture and Agronomy* (Cambridge, MA: Academic Press, 2023), 321–352, <https://doi.org/10.1016/B978-0-323-91809-1.00016-0>.

36. V. Romanovski, “Positive and Negative Effects of Different Metal-Based Nanoparticles on Seed Germination and Plant Growth,” in *Nanofertilizer Delivery, Effects and Application Methods* (Amsterdam, Netherlands: Elsevier, 2024), 251–270, <https://doi.org/10.1016/B978-0-443-13332-9.00006-X>.

### **Supporting Information**

Additional supporting information can be found online in the Supporting Information section.